SAND2013-0564C

LNG VESSEL CASCADING DAMAGE STRUTURAL AND THERMAL ANALYSES

Jason P. Petti, , Carlos Lopez, Victor Figueroa, Robert J. Kalan, Gerald Wellman, James Dempsey, Daniel Villa, Mike Hightower

Sandia National Laboratories
Albuquerque, New Mexico, USA

Keywords: Cascading Damage, Cryogenic Fracture, Fracture Testing, Flow Analysis, Finite Element Analysis

I. Introduction

The combination of the potential for the expansion of future imports and exports of liquefied natural gas (LNG) from or to the U.S. along with the increased safety and security concerns resulting from the incidents of September 11, 2001, have led to an exploration of the impact an attack on an LNG ship would have on public safety and property. The US Department of Energy (DOE) has funded several studies (Hightower, et al., 2004, Hightower et al., 2006, Luketa et al., 2008, Kalan et al., 2011, Figueroa et al., 2011, and Petti et al., 2011) that have examined the potential hazards from an accidental or intentional breach of an LNG cargo tank and the potential for cascading damage. Here, cascading damage is defined as damage caused to the LNG ship or cargo tanks from an initial spill that would lead to the subsequent release of LNG from additional cargo tanks. In 2007, the US Government Accountability Office (GAO) produced a report on LNG research and identified several areas where additional research was suggested. Improving the state-of-knowledge surrounding the potential for cascading damage to LNG ships was among the most critical needs. The study of cascading damage issues has proven difficult primarily due to the fact that these events require the analysis of the interaction of a series of complex physical processes (e.g., LNG flow, heat transfer, fire development, and structural fracture, damage and response). Consideration of cascading damage impacts are based on LNG vessel structural steels being extremely brittle at LNG temperatures (-161^{o}C), and LNG fires generating very high temperatures (exceeding 1000^{o}C) that will lower the strength of structural steels. This paper summarizes the more recent of these studies (Kalan et al., 2011, Figueroa et al., 2011, and Petti et al., 2011) which explored the cryogenic and fire thermal damage to an LNG ships during a large LNG cargo tank breach and the potential for cascading structural damage.

II. LNG Ship Cascading Damage Study Approach and Purpose

The efforts summarized in this paper examined the assessment of the susceptibility of an LNG ship and cargo tanks to cryogenic and fire damage from a large LNG spill. To accomplish this assessment, Sandia National Laboratories developed a comprehensive set of modeling and testing efforts focused on developing an understanding of LNG ship and cargo tank structural damage from cryogenic and fire hazards, which are of critical importance in determining the likelihood and the impact of cascading damage on public safety. For example, if cascading damage occurred and caused additional LNG to spill simultaneously with the initial spill, then significantly larger pool fires could occur and increase hazards, while if cascading damage did not occur, or if it only caused sequential spills of LNG, then the size of the initial spill and the hazards would likely not increase. To study the cascading damage potential and damage progression from an initial LNG cargo tank breach and spill event, a detailed step-wise testing, analysis, and modeling approach for each of the different physical processes were integrated into a system-level LNG ship and cargo tank damage, cascading damage, and hazard evaluation. The major elements of the LNG Ship Cascading Damage Study included:

- Conducting a series of high and low temperature ship structural steel material property tests for use in thermal damage modeling,
- Conducting a series of large-scale ship steel cryogenic fracture and damage tests to develop a detailed cryogenic fracture and damage modeling, and
- Using high-performance computing resources to model and analyze in detail LNG cargo tank breach, LNG spill and flow, assess cryogenic and fire thermal impacts, and assess cascading damage potential of an LNG ship and cargo tanks.

The LNG Ship Cascading Damage Study required the use of detailed LNG ship information and data that included ship and cargo tank configuration and dimensions, materials used and construction details, frame and stiffener spacing and location, and openings and connected passageways. This information was

required to accurately model credible breach sizes in cargo tanks from high energy impacts or threats (performed under separate studies, Hightower et. al., 2004, Luketa et al., 2008), better estimate LNG spill flow directions and quantities, and to conduct the detailed cascading and structural damage analyses.

For this study, two common classes of LNG ships, both Moss and Membrane LNG ships were examined. The Membrane LNG ship studied was a large-size, conformal, 5-tank , Qmax design, which carries ~260,000 m^3 of LNG. The ship is similar in design, layout, and construction to the slightly smaller and more common Qflex design, which carries ~215,000 m^3 of LNG, as well as some of the smaller Membrane LNG Ships used in the U.S. The Moss LNG ship studied was a moderately sized, 5-tank Moss spherical design, which carries ~140,000 m^3 of LNG. The sizes selected span many of the Moss and Membrane ships used in the U.S. today, including the largest LNG ship designs.

Detailed structural drawings of actual LNG ships were obtained for both designs through support and assistance from members of an external technical review panel. In order to make the analyses and conclusions reached in this study applicable to most of the LNG ships in use today, some minor geometric simplifications and symmetry assumptions were made in the ship modeling. As such, the analyses presented are not intended to represent a specific vessel, but rather should be considered as providing general trends for the structural response and damage for many LNG ships. The major dimensions and relative size of the Moss and Membrane LNG ships studied are summarized in Table 1.

Table 1. Dimensions of Moss and Membrane LNG Ships Evaluated

Dimension	Moss	Membrane
Length	280 m	330 m
Breadth	45 m	54 m
Depth	25 m	27 m
LNG Cargo Capacity	140,000 m^3	260,000 m^3

As mentioned above, the level of modeling detail varied depending on the application, whether for flow or structural analysis. In general, the mid-ship regions were modeled in more detail (assumed location of initial breach), while the fore and aft regions of the LNG ships were modeled with a lower level of detail.
The general geometric configurations of the Moss and Membrane LNG ships considered and their cross-sections are shown in Figure 1 and 2, respectively.

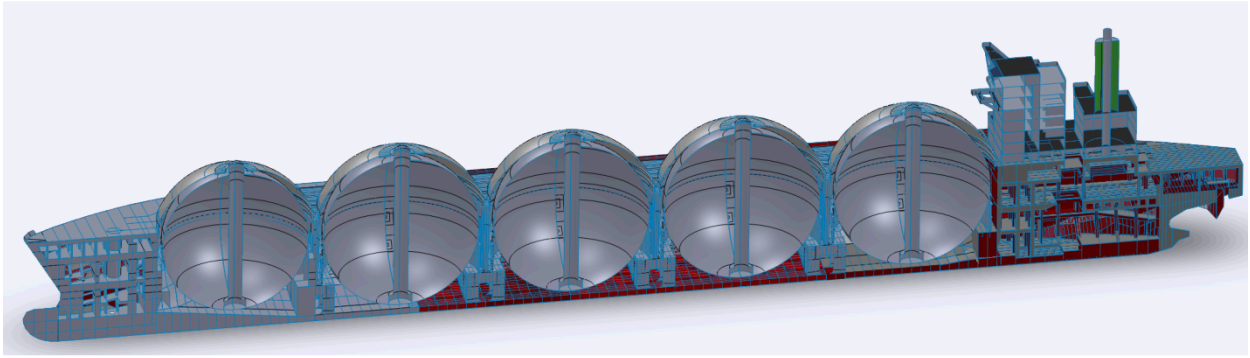

Figure 1. Moss LNG Ship cross-section

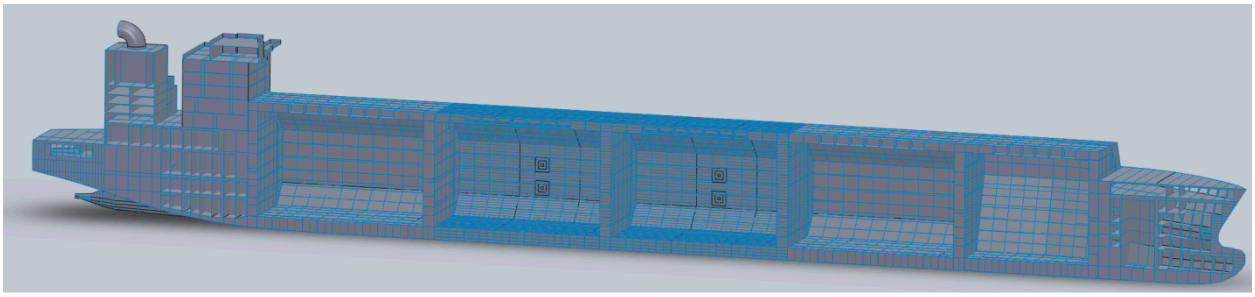

Figure 2. Membrane LNG Ship cross-section

III. LNG Ship Breach and Flow Analysis

Previous DOE directed studies of large LNG spills over water (Hightower et. al., 2004 and Luketa et. al., 2008) have explored potential accidental and intentional damage scenarios. These evaluations have considered a wide range of possible threats including accidents and intentional events. Potential credible events are site-specific, and vary depending on whether the marine transport is in an inner harbor, an outer harbor, or at an offshore Deep Water Port location.

For this study, Sandia focused on evaluating a range of credible breach sizes based on the previous studies of credible events. The nominal breach sizes selected were based on detailed, two and three dimensional, shock physics/structural damage models. The detailed results for these breach analysis efforts are not available for public release. However, Table 2 summarizes the range of LNG cargo tank breach sizes considered in Sandia's LNG studies. The larger holes ($5m^2$ to $15m^2$) were considered the most consequence significant and hence used in the LNG Cascading Damage Study. The holes were evaluated in the appropriate locations on ships (e.g., waterline, above waterline, midship, etc).

Table 2. LNG Cargo Tank Breach Sizes Considered

Type	Breach Area	Breach Dimension
Small	0.005 m^2	(0.25 feet square)
Medium	0.5 m^2	(2.3 feet square)
Large	3 m^2	(5.7 feet square)
	5 m^2	(7.3 feet square)
Very Large	15 m^2	(12.7 feet square)

In order to determine the extent of LNG flow during a breach event, three-dimensional computational fluid dynamics (CFD) analyses of the internal and external flow of spills from the Moss and Membrane cargo tanks were performed for the both the large and very large hole sizes. The flow analyses used breach dimensions noted above and assumed they extended through the outer and inner hulls of each ship and into an LNG cargo tank. The CFD analyses included the entire flow physics including the draining of the affected cargo tank, the flow and timing of the LNG flow internal to the ship, the LNG vaporization and migration during spills, and the amount of LNG that would spill outside the ships in order to estimate the size of the LNG pools that would be created on the water.

The commercially available code, CFD2000, was utilized to perform all flow modeling and spill analyses. CFD2000 is a general-purpose CFD program intended for complex scientific and engineering flow calculations (Adaptive Research, 2008). The CFD models and analyses include appropriate geometric, mesh, and boundary conditions. LNG vaporization was included for LNG-water and LNG-metal interface interactions. It uses a finite-volume formulation with advanced features of interest for this problem including; a free surface flow model to analyze liquid-gas and liquid-liquid flow inside and outside the ships, and an evaporation model to analyze liquid-gas phases. Since LNG boils at -161°C, significant LNG evaporation occurs when it comes into contact with the steel ship structures and water. The computational flow techniques used to analyze the LNG spills and flow are described in more detail in (Figueroa et al, 2011).

The CFD flow analyses showed substantial LNG flow inside and outside each ship for the larger breach scenarios. In the case of Moss ships, the design is such that LNG can pool underneath the cargo tank as shown in Figure 3. The LNG flow also extends from the cargo tank region to the double hull (e.g., ballast tank) compartments directly across from the cargo tank hole. Within approximately 30 seconds, widespread flooding occurs in the initial double hull compartments as well as initial flooding of the lower compartments through holes in the steel plating in the ballast tank region. In addition, the LNG has also begun to flow out to the water external to the vessel.

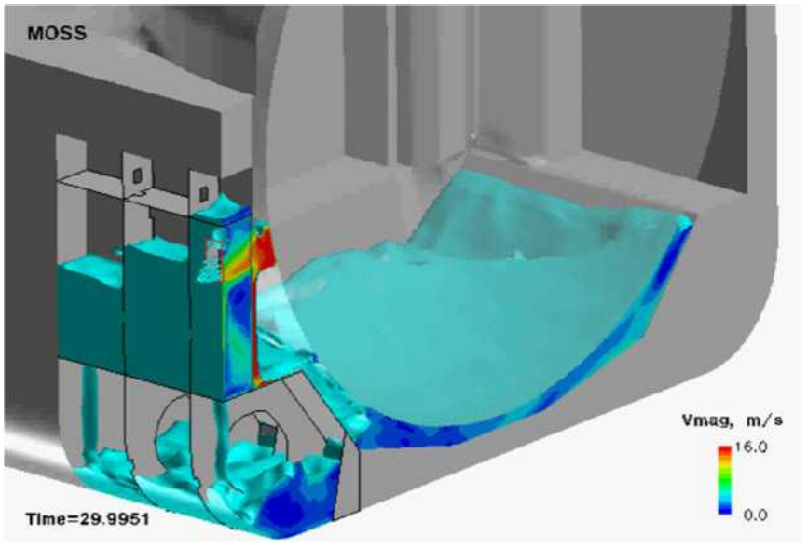

Figure 3. Moss LNG ship spill and internal flow analysis example

Similar results were obtained for the other hole sizes for the Moss ship and cargo tank designs. While the general trends identified were similar for most cases, the timing and distribution of LNG flow onto the water surface and inside the LNG ship vary, which impact the general timing of ship cryogenic damage and pool fire sizes and hazard distances.

For the larger breach events of the Membrane ships, less internal LNG flow was observed since the Membrane cargo tank is integral with the inner hull. Therefore, a breach in a cargo tank flows directly into the double hull compartments (e.g., ballast tank) and directly outside to the water. The internal structure of Membrane ships is essentially symmetrical longitudinally along the keel with no penetrations or flow paths across the ship centerline. Therefore, a breach and flow only impact one side of the vessel, which helped minimize the CFD flow analysis needs. Figure 4 shows an example flow analysis of LNG flow from a Membrane ship cargo tank. LNG flows out of the cargo tank and proceeds into the double hull compartments. LNG then begins to flow to the adjacent compartments and eventually begins to flow into the lower sections as flow paths allow. Since the LNG flow volume is spread across a large number of compartments within the double hulls, the time required to flow into and fill these compartments is slightly longer than observed for the Moss ship designs. As with the Moss, LNG also flows out of the vessel forming an LNG pool external to the ship.

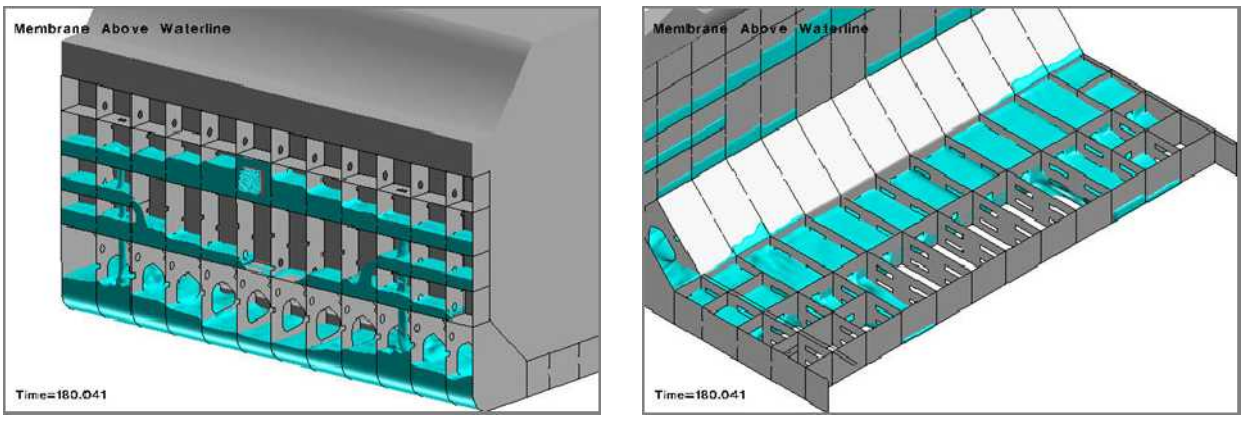

Figure 4. Membrane LNG ship spill and internal flow analysis example

For both the Moss and Membrane LNG ships, after a large breach event, LNG begins to flow both out onto the water as well as into double hull compartments and cargo tank areas. As the internal compartments and spaces begin to fill with LNG, more of the LNG will flow out onto the water surface.

Figure 5 shows examples of LNG spill analyses for Moss and Membrane ships, showing estimated flow timing, duration, and pool sizes for one of the large LNG cargo tank breach and spill events. These values therefore provide an estimate of the size of the LNG pool fire that could be expected from a large spill.

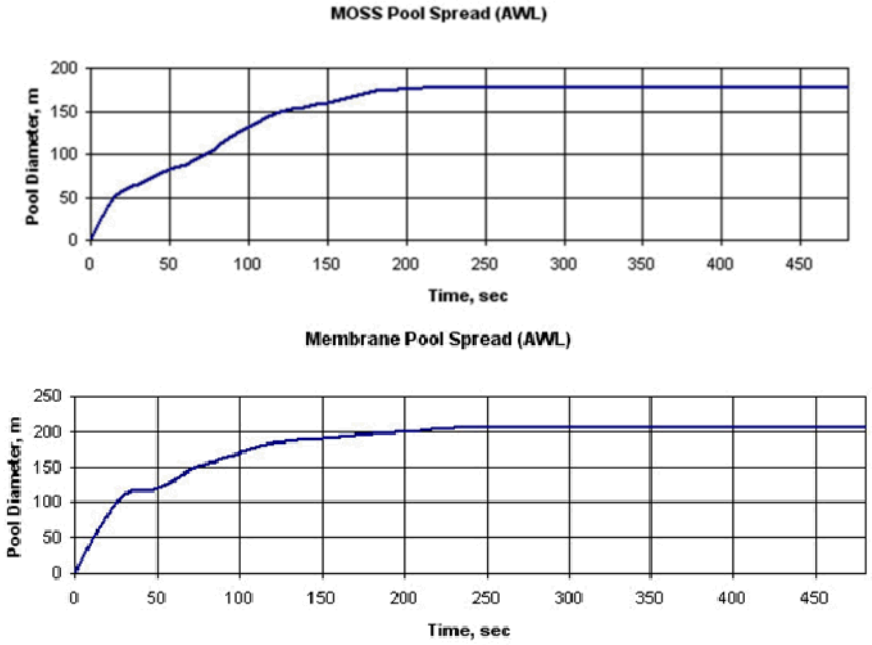

Figure 5. Example of LNG pool spread on water for a large spill

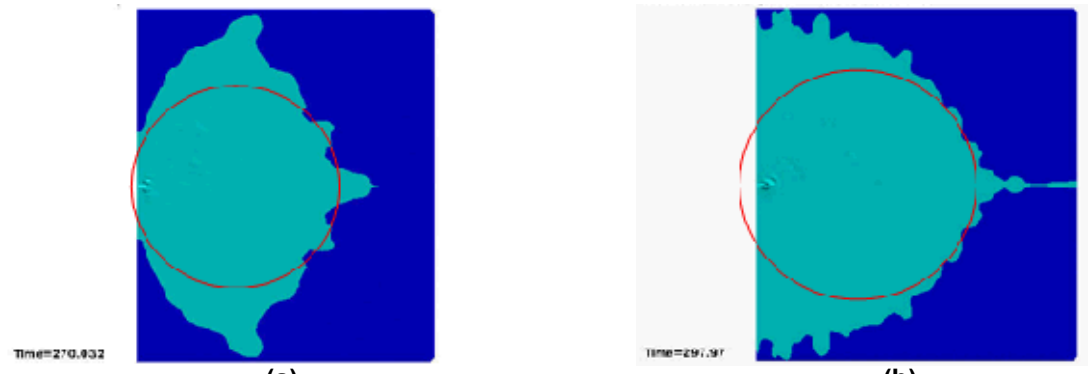

Figure 6. Example of LNG pool spread: (a) Moss ship with a 180 m diameter pool, (b) Membrane ship with a 210m diameter pool. (The LNG ship breach is on the left side)

Figure 6 highlights two LNG pool configurations calculated with the CFD2000 model. While the pools are not exactly circular, assuming circular pool sizes, as shown with the inscribed circles, give a reasonable estimate of pool sizes for fire hazard distance estimates.

The flow analyses conducted for this study show that for the larger breach events, as much of 40 percent of the LNG will likely flow into the LNG ship. The spill and flow analyses show that the internal flow of the LNG in a Moss ship will be completed within ten and fifteen minutes, at which time the LNG will all flow out onto the water. For a Membrane ship, LNG flow into the ship will be completed in about 10 minutes, and then the LNG will flow out onto the water. The results for the external flow analyses show that for the various breach events and ship designs, pool diameters of between 180 m to 350 m for the Moss, and between 200 m to 330 m for the Membrane LNG ships are generally expected for the larger breach events.

The flow modeling analyses were designed to provide information that could be used to directly support cryogenic and fire hazard and cascading damage modeling. The results from the internal flow analyses were used to identify the regions and timing of cryogenic LNG flow within the ship structures. Results from the

external flow analyses were used to identify the diameters of the LNG pools outside the vessels for each breach and spill event considered, and were used in subsequent fire analyses to identify regions of the vessels affected by the pool fires.

IV. LNG Ship Steel Material Testing, Large Scale Fracture Testing, and Damage Model Development

While the previous section described the LNG flow analysis, a series of material tests and large-scale fracture tests were conducted to assess the response of the LNG vessel's steel structure to LNG flow and fire. Structural steels are susceptible to low temperature brittle fracturing and high temperature softening. Figure 7 shows examples of cryogenic fracturing of LNG ship steel deck plates that have occurred from relatively small LNG spills.

Figure 7. Example of cryogenic damage of steel ship decks from LNG spills

In order to predict the thermal (both cryogenic and high temperature) structural cascading damage response of the ships, testing was required on ship structural steel materials to determine the material behavior at extreme temperatures (from -161°C for cryogenic LNG temperatures and up to 1000°C for LNG fire temperatures). The two LNG ships being considered use numerous American Bureau of Shipping (ABS) steel grades (e.g. ABS Grade A, B, D, E, AH32, etc.). Therefore, a series of material property and material failure tests were performed on two ABS steels that are representative of the structural steels used in standard LNG ship construction. The two steels selected were ABS Grade A and ABS Grade EH. The Grade A material reflects the lower strength and fracture toughness ABS steels, while the Grade EH represents the higher strength and fracture toughness steels. The testing of these two materials enabled a bounding of the response of the range of steels found in LNG ships.

Tensile, coefficient of thermal expansion, and Charpy v-notch tests were conducted over a temperature range that spanned from -191^{o}C to 800^{o}C (82^{o}K to 1073^{o}K). The low temperature (-191^{o}C) was chosen because it is the temperature of liquid nitrogen used in the large-scale fracture testing. Liquid nitrogen is slightly colder than LNG, but allows for safer test conditions. The high temperature limit (800^{o}C) was chosen due to concerns about oxidation of the specimens that could degrade mechanical property information, activation of creep and diffusion deformation mechanisms that could lead to time dependent behavior, and other concerns. Actual hydrocarbon fires can reach higher temperatures, exceeding 1000^{o}C, however thermal conduction paths into the ship structure make it unlikely that many structural elements other than the outer hull would reach temperatures that high.

Round bar tensile test results were the primary material response data used to measure material properties for use in response models, and were conducted following American Society for Testing and Materials (ASTM) standards. The ABS Grade A round bar tensile test data are shown in Figure 8, and ABS Grade EH round bar tensile test data are shown in Figure 9. For the ABS Grade A material at low temperatures, the expected increase in strength with reduced temperature is observed. There is no significant reduction in ductility for any temperature between 23^{o}C and -161^{o}C. However, at -191^{o}C, the response is brittle with no apparent plasticity even in the absence of any recognized dominant flaw. The ABS Grade A steel shows an increase in strength and a decrease in ductility at 200^{o}C and 300^{o}C. At 200^{o}C, there is also evidence of serrated plastic flow. These effects are consistent with dynamic strain ageing, which is not uncommon for

this class of steels in these temperature ranges. At 400°C and above, the expected decrease in strength is observed. Ductility increases with decreasing strength as expected until 800°C, where the ductility is reduced from that seen at 600°C but is still greater than at room temperature. Overall, there were no surprises in the tensile test results for the ABS Grade EH material. At low temperatures, ABS Grade EH showed an increase in strength and a reduction in ductility as expected. At elevated temperatures, ABS Grade EH showed the expected decrease in strength and increase in ductility. Dynamic strain ageing was not apparent from the tensile test results on the ABS Grade EH material.

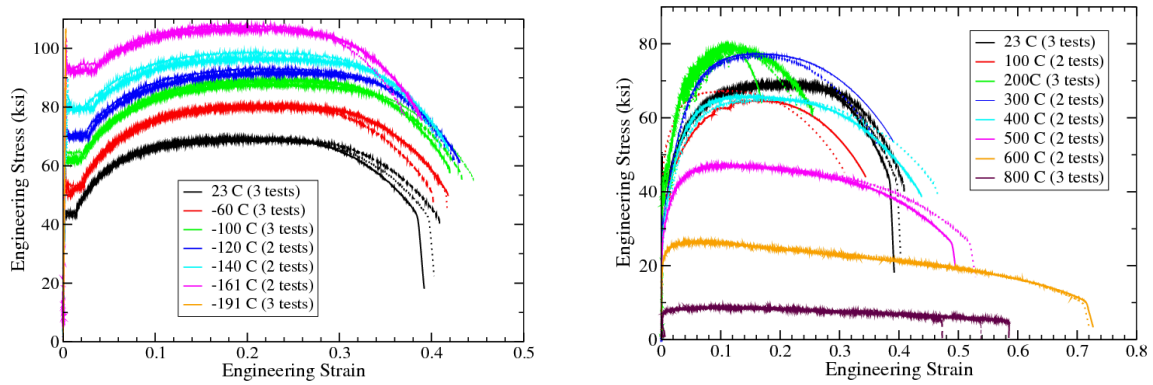

Figure 8. Tensile test results for ABS Grade A steel at low and high temperatures (MPa = ksi * 6.895)

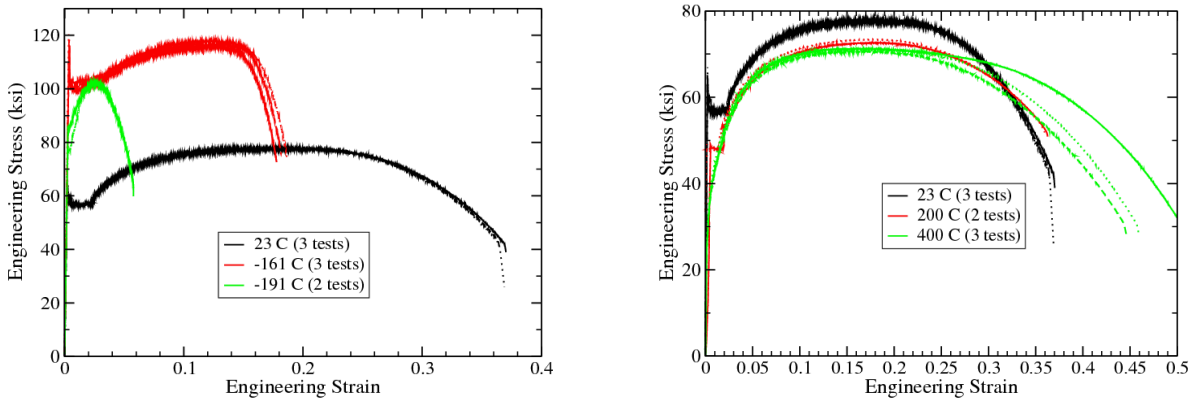

Figure 9. Tensile test results for ABS Grade EH steel at low and high temperatures (MPa = ksi * 6.895)

In addition to tensile testing, Charpy V-Notch testing was performed from -191°C (far below the brittle transition region) to -24°C (above the brittle transition region) for both ABS steels. The Charpy V-notch energy absorption test results are shown in Figure 10. There are several methods of estimating the fracture toughness from Charpy V-notch energy absorption data. A correlation (Rolfe and Novak, 1970) was used that is appropriate for the lower shelf and lower transition region of the Charpy curve. This produces an approximate lower shelf fracture toughness of 21 $ksi\sqrt{in}$ (23 $MPa\sqrt{m}$). The fracture toughness for both materials is very low at temperatures below -100°C, which is still well above the cryogenic temperature of LNG.

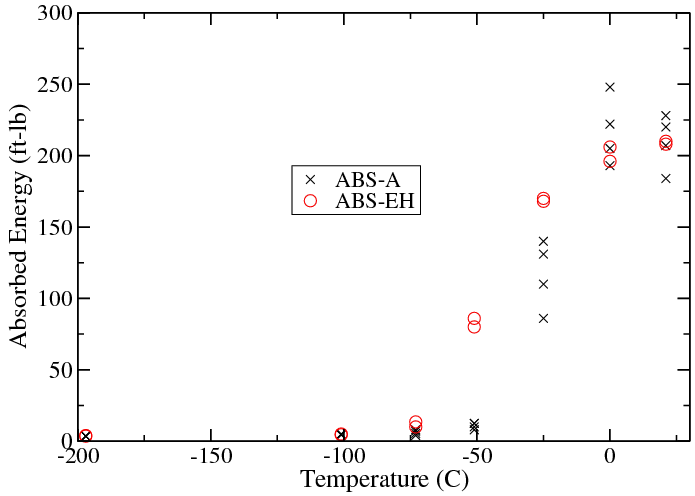

Figure 10. Charpy V-Notch energy absorbed for ABS Grades A and EH steels (Joule = ft-lb * 1.356)

The basic material tests provided initial estimates needed for modeling the material behavior. However, a series of large-scale fracture tests (Kalan and Petti, 2011) were required to further calibrate and then validate the damage model needed for modeling the full vessel behavior. The assessment of the ships was accomplished through a series of computational finite element analysis of models of each LNG ship. The models created for these analyses are relatively large; however, the analyses were capable of characterizing the material response on elements, the smallest of which are approximately 4 inches by 4 inches (100 mm by 100 mm). While this level of resolution provides sufficient stress/strain analysis to capture the global behavior of the vessel, this scale is several orders of magnitude too large to capture the stress/strain fields that may be generated at the tip of a crack in the steel that comprises the hulls of LNG tankers when subjected to thermal stresses resulting from contact with the cryogenic LNG. In addition, the progression of brittle cracks in steel plates depends on a number of factors including the specific geometry, the material properties, the temperature state caused by contact with cryogenic liquids, and the microstructure of the material. Specifically, the dependence on the microstructure of the steel plating from point-to-point makes it impossible to predict the individual brittle crack behavior using continuum mechanics in finite element models. However, specific knowledge at the microscopic level of detail is not necessary to assess the global behavior of the ship. What is necessary is an approximate estimate of the general crack path and directionality. The “damage” caused by cracks will be represented in the finite element models by the failure or “death” of a path of 4 inch by 4 inch elements. The “death” of a finite element is achieved by removing that element from the analysis after a defined criteria has been reached for that element, causing material separation. For these analyses, a strain/temperature locus is employed as the failure criterion (e.g., damage model). Due to the transition from ductile to brittle behavior as the temperature drops, the strain required to “kill” a finite element drops drastically as the temperature falls. The temperature at which the strain drops most dramatically varies from steel to steel; however, all of the marine steels used in LNG tanker construction enter the brittle regime at temperatures well above LNG temperatures. The initial strain/temperature locus was developed using basic material tests (tensile tests at multiple temperatures). The large-scale fracture test results were used in the secondary calibration and validation of the strain/temperature locus.

The structural fracture test series were designed to induce large thermal stresses in the test plates due to differential thermal contraction while simultaneously lowering their ductility. As previously discussed, liquid nitrogen (LN2) was chosen as the cryogenic fluid for testing. It is significantly safer to work with and the temperature of LN_2 is slightly colder (-190^{o}C) than LNG (-161^{o}C). The use of LN2 ensures that the tests could achieve temperatures in the range an actual ship would see during an LNG spill. There were four phases in this test series. Phase I was an initial exploratory stage that provided preliminary data to steel material response to LN2 (LNG) and insight and direction for the series of larger scale tests. In the Phase II series of tests, larger plates were used, ranging in size from 4 ft square pieces to 6 ft square sections. This phase investigated the cooling rates on the plates and the effect of different notch geometries (stress concentrations were machined into the test articles to initiate brittle fracture) from which a crack would initiate. Phase II was broken in to two sections, Phase II-A and Phase II-B. Phase II-A used standard A36 structural steel, while Phase II-B used marine grade steels. In Phase III, significantly larger 12 ft square

structures with more complex geometries were tested. The final test phase, Phase IV, investigated the heat transfer (cooling) rate differences between LNG and LN_2.

Figure 11. Example Phase II Test Article

Two fracture tests used for damage model calibration are shown in Figures 12 and 13 as examples of these efforts. In these figures, regions colored blue have a temperature less than -90.5°C. The red material has a temperature greater than 14.5°C, and white indicates an analysis calculated crack. The first test used ABS Grade A steel with a cooling region of 40 inches by 12 inches. The experiment created a crack approximately 12 inches long across the narrow dimension of the cooling region. The crack propagated perpendicular to the dominant principle stress direction. The strain-to-failure, as a function of temperature, was evaluated to determine the required modifications to the strain/temperature locus to give the same crack length and directionality. Cracking in this location and in this direction is controlled by the stresses produced by the cooling and is very repeatable. The entire test specimen geometry is shown for the analysis to allow for orientation of the reader. Only the crack (approximately 12 inches long) is shown in the picture of the experiment.

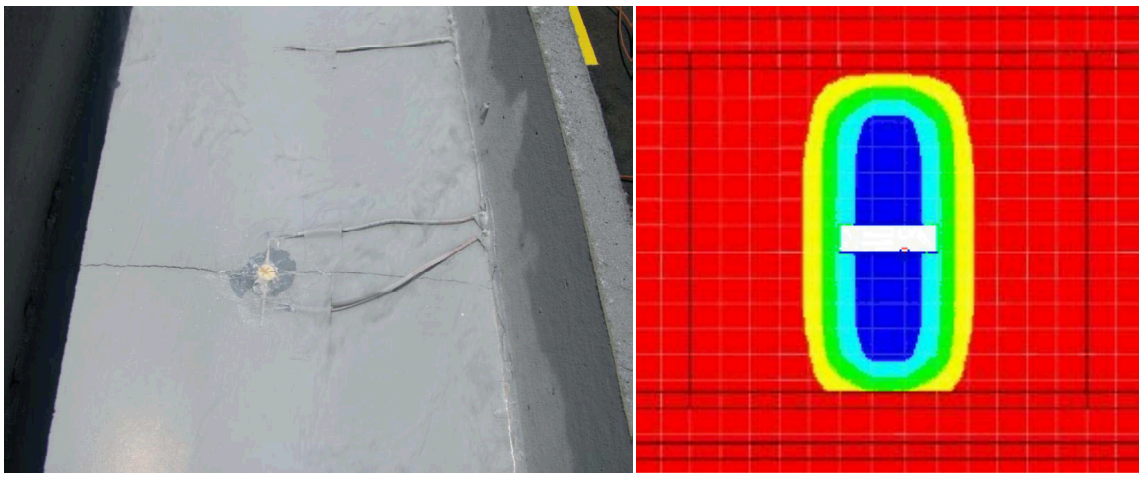

Figure 12. Comparison of test and analysis for an initial damage model calibration

The second calibration test shown in Figure 13 is similar to the first test, with all elements colored blue having a temperature of less than -109°C, and red indicates temperatures greater than 3°C. The material was again ABS Grade A. The cooling region was defined by a region size of 30 inches by 24 inches. As with the result of the first test example, the crack propagated across the 24 inch narrow dimension of the cooling trough, again perpendicular to the dominant principle stress direction. However, here the crack bifurcated in different directions on the two edges of the 24 inch region. This bifurcation makes sense in that the stress state is much more bi-axial than in the first test. The damage model also suggested the bifurcation, though slightly different with a less complex shape than in the test due to the large element size. However, the change in direction of the crack shown in the analysis is indicative of the model reflecting the

bi-axial stress state in the structure, and therefore can provide good estimates of fracture and damage based solely on material properties, configuration, and the loading and thermal stress state.

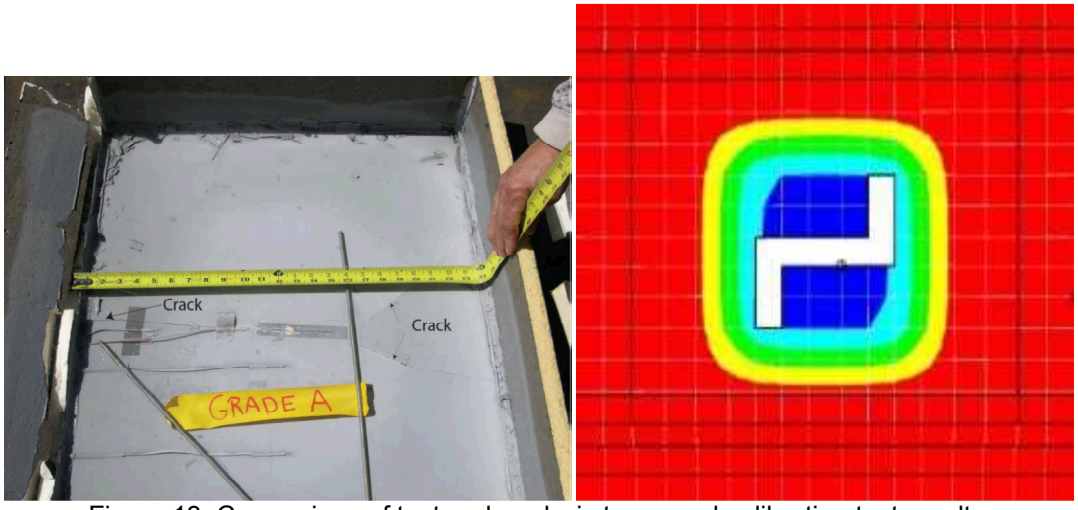

Figure 13. Comparison of test and analysis to second calibration test results

In order to provide validation of the modeling technique and the parameter estimation, larger, and more complex test specimens were fabricated and tested in Phase III with an example shown in Figure 14. As with the Phase II tests, a notch was introduced to facilitate fracture. A finite element model of the test structure was also constructed using 4 inch elements, and the cooling was produced through a heat transfer analysis to drop the temperature in the region cooled in the test. The experimental cracking was compared to the computed element failures as shown in Figure 15.

Figure 14. Phase III Test Structure

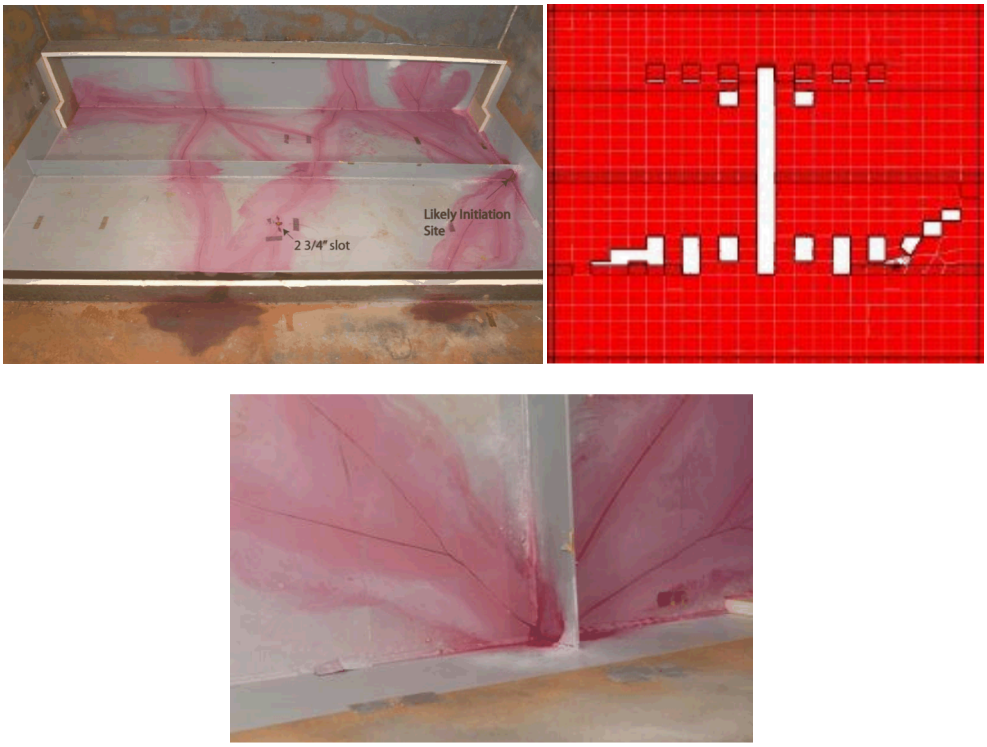

Figure 15. Comparison of damage analysis to experimental test results (top) and crack initiation site (bottom)

Again, the crack pattern from the analysis does not exactly match the experiment; however, as was the case for the other experimental comparisons, the extent of cracking and the general direction of cracking is quite similar to the calculated damage and fractures. Figure 15 also illustrates the initiation site for the Phase III test shown. The fracture initiation site for this test occurred at a geometric detail (e.g., the intersection of a stiffening element and two adjacent plates). The smaller Phase II tests required a notch to be machined into the plates to initiate fractures. As the geometry becomes more complex, as would be the case in an actual LNG ship, the number of stress concentrations capable of initiating fractures increases dramatically.

The calibration and validation of the damage model was limited by the number of large tests that could be conducted. The testing conducted and damage analyses performed were designed to develop a failure modeling technique that would provide a good qualitative estimation of damage progression on ship steels as the result of a spill of LNG. The similarity between the experiments and analyses in the extent and direction of cracking suggests that the fracture model and analysis technique can provide a satisfactory estimate of cracking and damage when applied to a full ship structural model.

The last test series was designated Phase IV and examined simple steel plates subjected to both LNG and LN2 to assess any differences in cooling rates. These tests showed that in general LNG cools more effectively than LN2. The appropriate cooling rates were then used in the LNG ship modeling described below. Additional details on these cooling rate tests are provided in Kalan et al. (2011).

V. LNG Ship Damage Modeling

This section provides a summary of the development of detailed high performance computing structural analysis models, the cryogenic and fire thermal loading approaches used to identify the time-varying thermal stress states on the ship structure, and results of the overall ship structural damage analyses. These results are presented in detail in Petti et al. (2011) and Figueroa et al. (2011) (however both reports are available only to appropriate government agencies and researchers).

From the LNG ship geometric models developed, a finite element structural analysis model was created for both the Moss and Membrane LNG ships being evaluated. For the structural analyses conducted, elements with 0.1 m (4 inch) edge lengths were used in the regions where cracking could potentially occur. The

smaller the element size, the greater the resolution of overall stresses and strains. While elements smaller the 0.1 m would provide more resolution, they would also increase the size of the model and increase the complexity and computer requirements for each analysis. In regions outside of the areas of potential cracking, the mesh size was gradually increased to a maximum of approximately 1 m, with most in the 0.3 m to 0.5 m range.

This approach produced two structural models, each with between four and five million elements. As shown in Table 3, more than 70% of the total elements are in the mid-ship region where the breach and fracture damage were assumed to occur. The Moss geometry and mesh are considerably more complex due to the large number of circular intersections associated with the spherical tanks. This helped contributed to the Moss model having more elements. Figure 16 and Figure 17 show examples of the mesh details for the Moss and the Membrane ship finite element structural models.

Table 3. Moss and Membrane LNG Ship Structural Model Elements

Dimension	Moss	Membrane
Midship	3479100	3140900
Total	4877500	4278100
% in detailed region	71	73

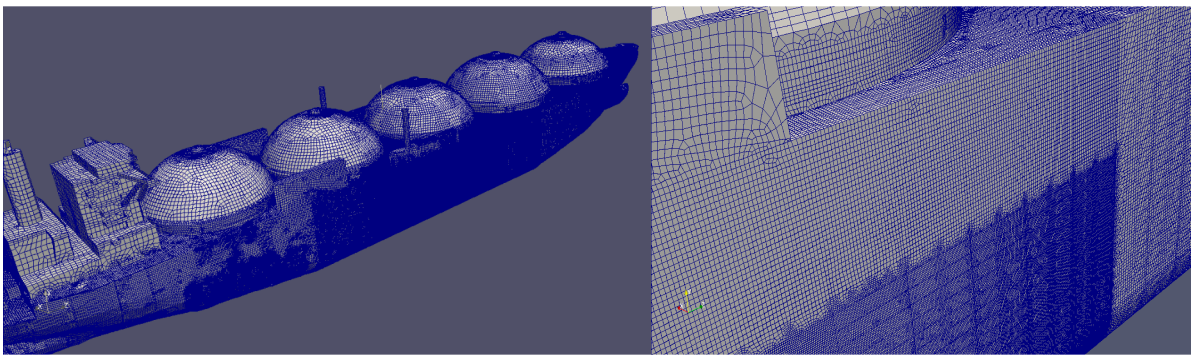

Figure 16. Moss LNG ship finite element structural model (left) and detailed region (right)

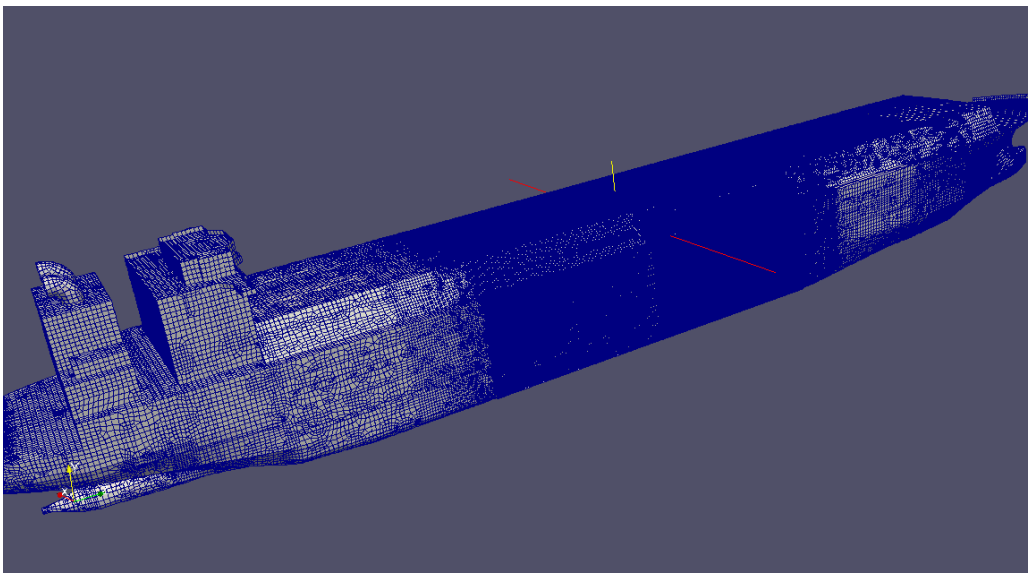

Figure 17. Membrane LNG ship finite element structural model

While accounting for the simplifications made in some regions, the thickness of the steel plating and material densities were assigned to various sections of the vessels. The models created in this study include all, or most, of the structural components. However, the vessels also contain many non-structural items including LNG cargo, cargo tank insulation, piping, machinery, anchors, fuel, water, etc. In order to account for the mass of these items in the models, the density of the steel of the plating was increased near their location. Particular attention was paid to the distribution of mass along the length of the vessels to make sure that the models provided the appropriate draft and stresses for normal operational load conditions. The load imparted on the structure by the LNG cargo was not distributed into the steel structure by increasing the density, but rather was applied by a hydrostatic pressure loading within the cargo tank regions of the models.

The cryogenic nature of LNG will cause the regions of the ship contacted by spilled LNG to reduce in temperature. To calculate the thermal temperatures of the structural steels, it is necessary to estimate the proper cooling rates to be applied to affected regions of the ship for the structural and damage timing and the final cascading damage potential. As indicated in the flow results, LNG can flow and collect in regions of the ship that are above and below the waterline. Since the outer surface of the outer hull of the vessel is exposed to air above the waterline and to water under the waterline, it was necessary to estimate the proper cooling rates for both of these conditions.

For the internal and external regions of the LNG ships that come into contact with the spilled LNG, they can be cooled by applying a simplified temperature decrease or cooling rate to the appropriate finite elements in the full-ship structural analysis models. The appropriate cooling rates used were based on experimental cooling rate data obtained from the Phase IV cooling rate tests described previously. The temperature response of the test plates was used to estimate the overall heat transfer coefficients using an inverse heat conduction technique. Forward problems were then run to find a constant heat transfer coefficient value that would estimate the temperature response of the test plates reasonably close to what was measured. These supporting analyses lead to an estimation of lower and upper bound constant heat transfer coefficients (400 and 1080 W/m^2-K). Subsequent analyses then determined that regions identified from the flow analysis that come into contact with the spilled LNG will reduce in temperature from 20^{o}C to -148^{o}C in at most 600 seconds (or 10 minutes).

For the external hulls of the LNG ship that have LNG flow internal to the vessel but have seawater on the other side, an additional analysis was required. The cooling rates were determined using a finite difference heat transfer analysis with Euler explicit time stepping. The analysis calculated ice growth on the water side of the external hull for each time step depending on the water/ice or water/ship interface temperature. At interface temperatures below the freezing point of seawater (-1.9°C), the analysis allowed ice to accumulate. Properties for seawater were based on a salinity of 35 g/l. For a case with a reasonable external current velocity (1 knot, 0.5 m/s) and for a wide range of bulk seawater temperatures, sufficient ice was determined to form and act to insulate the outer hull. This allows the outer hull to drop to temperatures approaching the temperature of the LNG over a period of time. Thus, the steel was determined to be cooled by the LNG at a similar rate as the case where air is on the outside of the hull. This supported the use of nominally the same cooling rates for regions above the waterline and below the waterline contacted by LNG. Since the water flow speed is important, site specific currents should be considered since they could potentially reduce ice formation and possibly the rate of outer hull cooling.

The flow analysis section discussed external flow estimates of the size of an LNG pool that would form adjacent to the ship. Since LNG also has a low boiling temperature relative to the temperature of sea water, boil-off will occur at the surface of the water releasing a mixture of flammable gases into the air. Therefore, the potential for a fire immediately outside the ship will exist. LNG burns at temperatures of about 1500°C, which could impact the structural integrity of the ship if a fire occurs for a significant period of time.

The spill results showed maximum pool diameters for medium to large spills of approximately 200 m to 350 m for the Moss and Membrane LNG ships. Using these pool diameters, pool fire analyses were conducted to estimate the thermal heating rate of the ship structural steel as input for the ship high temperature structural damage analyses. Fire analyses were conducted using computational fluid dynamics (CFD) models to help identify the regions of the ships affected by a pool fire. Fuego, a massively parallel CFD fire code developed and used by Sandia, was used to conduct all fire-structure interaction modeling aspects of the fire analysis. In Fuego, the fire flow field is solved by using a turbulent, low-Mach, incompressible form of the Navier-Stokes equations along with the conservation of mass for the mixture and individual species, and the energy equation. The primary use of Fuego was to estimate the envelope of the fire over the vessel.

A wind speed of 9 m/s (20mph) was used for these analyses and it was assumed directed toward the LNG ship. Figures 18 and 19 show the fire simulations and the affected portions of the Moss and Membrane

ships for the smaller pool sizes predicted for the larger LNG spills. In both cases, the fire impact extends beyond the diameter of the pool along the length of the vessel due to radiation and the wind makes the fires lay over onto each ship. The boxed region shows where significant heating is expected to occur, which includes the sides and tops of the LNG ships.

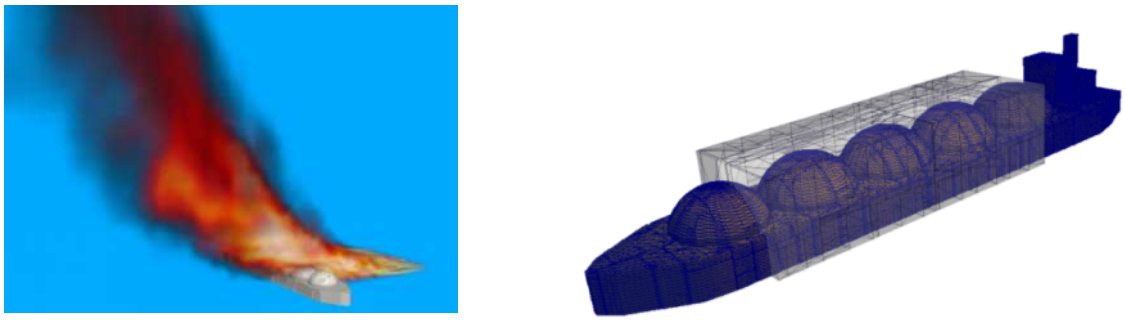

Figure 18. Fire impacting the Moss ship (left) and extent of heated region (right).

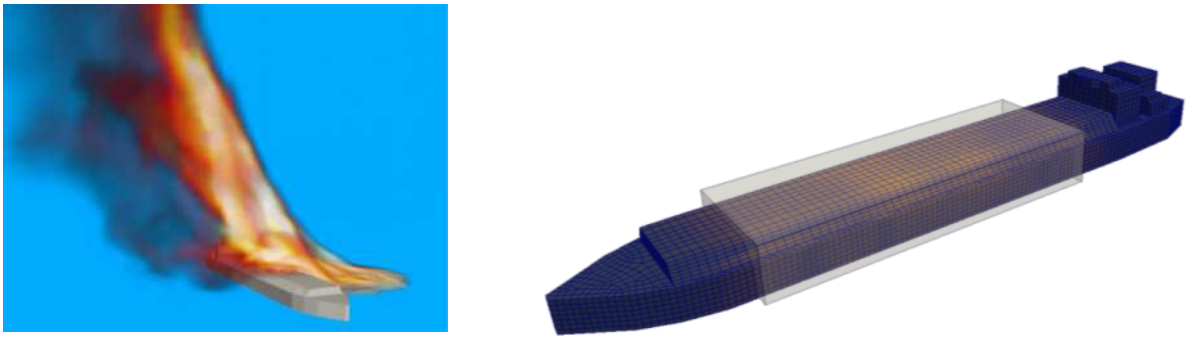

Figure 19. Fire impacting the Membrane ship (left) and extent of heated region (right).

The surface emissive power or heat rate obtained from the large LNG pool fire experiments (Blanchat et al., 2010), were used to define the LNG ship heating rates and heating regions to be used in the structural damage analyses.

Similar to the method used to establish the cooling rates, a combination of testing and analysis were used to determine the heating rates of the ship hulls as inputs to the structural thermal damage model. In this case, a half-symmetry model representative of the outer and inner ship hulls was created in the finite element code MSC PATRAN/Thermal. Based on the data from the large LNG pool fire experiments (Blanchat et al., 2010) and insulation testing (Blanchat, 2011), a surface emissive power of ~290 kW/m^2 was used to estimate the heating rate on the outer hull, which in turn heated the inner hull by radiation heat transfer. The heating was applied to the fire impacted regions of the LNG ships as determined from the fire modeling analyses from an LNG pool fire. The purpose of the simulation was to obtain information on representative maximum temperature responses of the inner and outer hull of an LNG ship exposed to a large LNG pool fire. A fixed "water" temperature was assumed below the waterline on the exterior surface of the outer hull.

The applied heating stayed relatively localized to the region it was applied to even after 30 minutes of simulation. This localized response is similar to what was observed in the cooling rate simulations. From these analyses, the temperature of the outer hull is expected to reach approximately 1325^{o}K (1000^{o}C), while the inner hull reaches approximately 1050^{o}K (775^{o}C) within approximately 15 minutes. Based on the flow of LNG and the size of pool, the fires are expected to last between 20 and 40 minutes. This analysis compares favorably with heating tests that were conducted to look at insulation damage (Blanchat, 2011).

VI. LNG Ship Damage Analysis Results

The LNG ship structural damage analysis and assessments employ finite element models, the material properties measured and cryogenic damage models developed, the cooling and heating rates measured, and the timing of the cooled and heated regions from the LNG flow and fire analyses to develop estimates of the timing and extent of damage of both LNG ships. From the spill and flow analyses conducted, the large to very large breach events give very similar overall LNG flow within the ship structures, with the major difference being some minor variation in the timing of the cooling of different regions. For this reason, a single detailed structural damage analysis was performed for each type of LNG ship.

For the analysis of both of the LNG ships considered, the gravitational loads, exterior seawater hydrostatic loads, and internal LNG cargo tank hydrostatic loads were applied to the ship structural models to first obtain the initial stress states of the vessels. ABS Grade A and EH steels were used to model the structural steel in each ship. For regions using lower fracture toughness materials (ABS Grades A, B, D, and E) ABS Grade A properties were used, and in regions using higher fracture toughness materials (ABS Grades AH32, AH36, DH32, DH36, EH32, and EH36) ABS Grade EH properties were used. This was done to simplify both the structural testing and data needed and the model input and quality assurance checks.

The initial load condition chosen to consider the initial stress states was the Summer Arrival Condition. For this condition, the LNG cargo tanks are 97% filled for the Moss and 98.5% filled for the Membrane. The draft for the Moss at this condition is 10.65 m (nearly constant draft at mid-ship, aft, and fore) and for the Membrane is 11.5 m (nearly constant draft at mid-ship, aft, and fore). After establishing the initial load and stress states and ship stability and draft of the structural analysis model for this condition, the temperature changes were applied to the structural models in accordance with the LNG flow and cooling rates discussed previously. These thermal changes changed the structural stress state and material properties of the structural steels such that cryogenic damage and the timing of that damage can be calculated using high-performance computational structural models.

For the Moss, the regions exposed to LNG flow were analyzed for cryogenic induced fracture. The LNG flow results were used to develop a series of regions of structural steel cooling that changed as the LNG flowed into the internal structure of the ship. Figures 20 and 21 show exterior and interior views of the ship's different regions that were cooled (blue and gray regions). The temperature and damage states within the ship were correlated with the LNG flow and cooling rate information. As discussed, no difference in cooling rate was assumed for the regions of the ship's outer hull above or below the waterline.

The flow analysis showed widespread LNG contact with steel plate surfaces within 30 seconds. Based on the extent of the flow and the cooling rates developed, the temperatures of the elements within the dark blue regions were decreased from 20^{o}C to -148^{o}C over 10 minutes. The light blue regions had their temperature decreased by the same temperature range and time, but the start of the cooling was delayed by 2 minutes. Finally, the gray regions had the temperature decreased similarly, but delayed the start of the cooling by 4 minutes. These delays were used to simulate the timing of the flow of LNG within the space surrounding the cargo tank for up to a cooling time of approximately 14 minutes. As shown in Figures 30 and 31, due to the design of the Moss LNG ships, the LNG flow from a breached tank remains within the ship structure surrounding the damaged cargo tank, and has few paths to move along the ship centerline into other cargo tank areas.

The analysis shown was initiated using an assumption that spilled LNG would not come into contact with the ship structure just above the bilge area. However, in many cases the LNG could come into contact with this area. Due to the long analysis time required for the first calculation, a second simulation was not conducted, but from the flow analysis conducted, the general state of damage can be easily estimated from the damage calculated from other regions cooled for similar times. The final structural damage results presented do include damage in the bilge area in estimating the worst case damage scenarios.

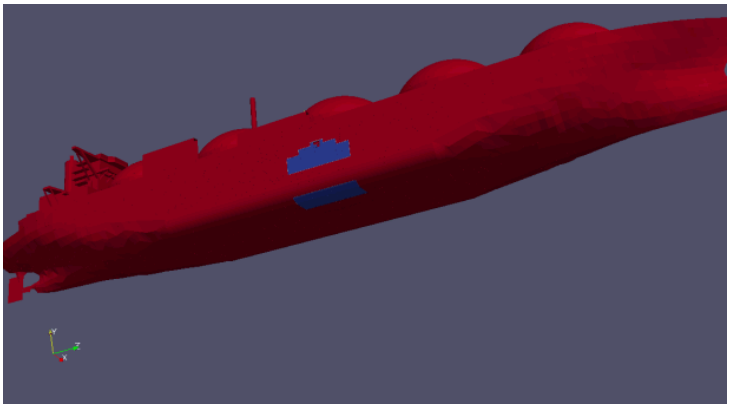

Figure 20. Moss exterior regions of temperature decrease

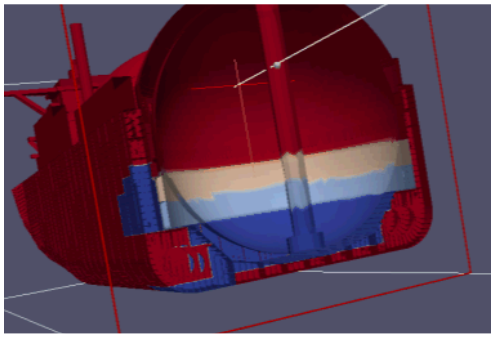

Figure 21. Moss interior regions of temperature decrease

As mentioned, the large to very large breach events provide generally similar LNG flows that were therefore similar in the extent of the cooling regions. The most significant differences were based on breach location, which alters the timing of the structural cooling and the eventual entrainment of seawater into the ship. In some credible breach events, significant water entrainment can occur within approximately 5 minutes. This could have several consequences. One plausible result could include the water displacing the LNG at the lower regions of the vessel below the waterline due to the higher density of water. This could minimize cooling and reduce potential structural damage. However, the mixing of LNG and warm seawater will cause a rapid vaporization of the LNG with potential pressurization, both of which could cause additional ship structural damage. These issues were considered in developing Moss LNG ship damage conclusions.

An example of the resulting cryogenic damage from a large to very large cargo tank breach and spill is shown in Figure 22. The white colored elements indicate the structural elements that reached the critical fracture damage strain criterion. The transparent view of the vessel shows both the cryogenic cracking and damage in the outer hull, and throughout the inner hull surrounding the cargo tank. The significant damage to the inner hull causes the outer hull to deform upward into the vessel as the hydrostatic pressure from the seawater is no longer resisted by the damaged ship inner and outer hull. The estimated displacement of the outer hull could be as much as 1 meter. The analysis predicts cryogenic cracking will occur throughout the portions of the vessel that were exposed to LNG flow. No damage was predicted to occur in regions outside where the LNG flowed and came into contact with the cryogenic LNG.

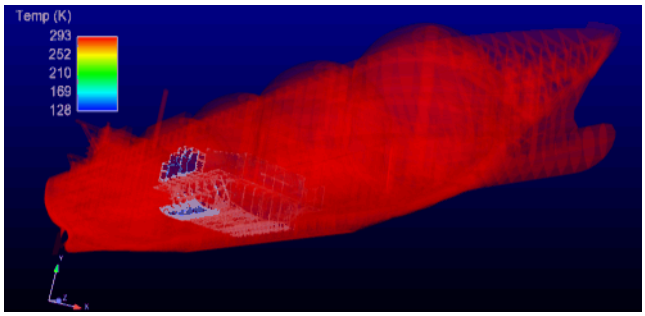

Figure 22. Example of Moss large LNG spill cryogenic fracture and damage

Because of the severe cryogenic structural damage calculated, including a significant number of killed elements and separation of regions of elements, the numerical structural damage model became unstable.

Therefore, assessing the final global ship deformation and response with this model after the cryogenic damage that was induced was simply not possible.

Based on the cryogenic structural damage analysis, much of the inner hull near a large breach event was damaged, reducing the ability of the vessel to resist hydrostatic loads from the surrounding seawater. In addition, the ship structural moment of inertia, or section modulus (the parameter that defines the ship's capability to resist bending loads and deformations) was drastically reduced, which impacts the ability of the ship to remain stable and afloat in the water. From the fire analysis, much of the ship structure near the fire on both the side and top of the ship could reach temperatures of between 775 and 1000°C for the inner and outer hulls. At these temperatures, the material properties of ship structural steels were shown from our testing to be severely weakened, having less than 25 percent of their original strength, and to deform significantly. Based on the cryogenic damage and weakening of the material exposed to the fire, the reduced plastic bending moment capacity for the Moss ship as a general function of time was developed as shown in Figure 23. The plastic bending moment capacity is defined as the bending moment that would lead to the entire cross-section of the ship yielding and creating essentially a plastic "hinge". The evaluation of the plastic bending moment capacity is often used in many extreme event risk analyses to more accurately predict the likelihood of overall structural system damage or failure during extreme events.

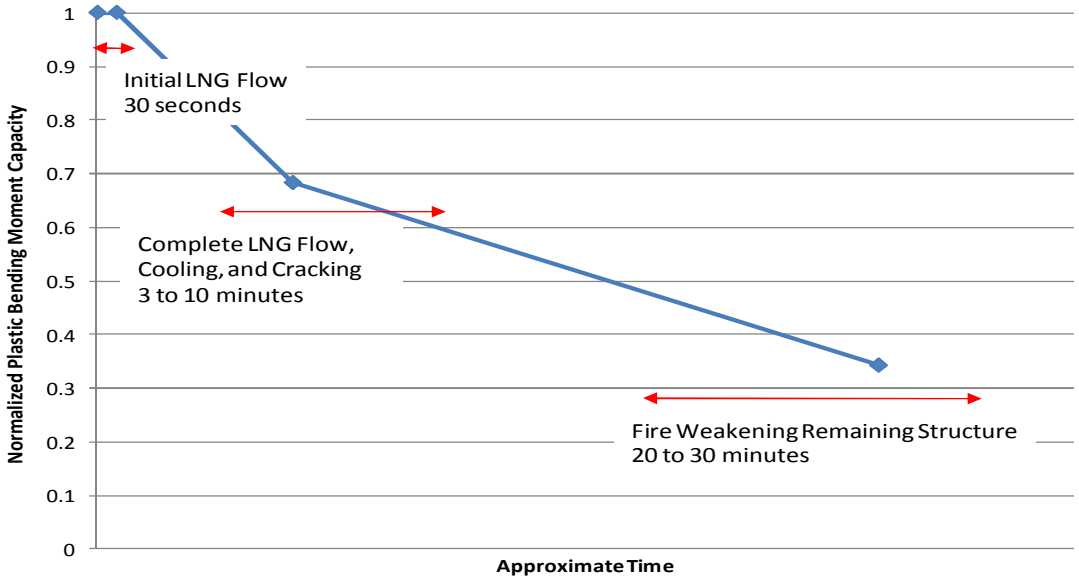

Figure 23. Moss ship reduction in plastic bending moment capacity for large spills

The moments are normalized by the full undamaged plastic moment capacity of the section. The cryogenic damage causes an approximate 32% reduction within 3 to 10 minutes with the fire causing an additional 36% reduction between 20 and 30 minutes. However, the reduction in the plastic bending moment capacity does not fully address the concern with the damage here. These capacity estimates assume that the cross-section is in a condition to obtain the full strength of the materials without section buckling. The damage to the inner hull reduces the remaining outer hull to a plate-like structure with a reduced capacity against buckling when in compression. In addition, the plating below the waterline has already been shown to have buckled inward due to damage and the hydrostatic pressure from the seawater. The initial loading of the vessel caused a "hog" condition which is also assumed to be the condition after the damage occurs (the center tank has drained significantly). This would place the remaining, and already, buckled outer hull below the waterline in compression. The sections of the inner and outer hull at the top of the ship are affected by the fire and have little resistance to tension. Therefore, the ship was judged to have essentially little remaining strength and to be overall disabled and severely damaged.

At this point, with no risk mitigation steps taken, the ship most likely will deform significantly or may separate at the region of the damaged cargo tank. However, if these events occur in an inner harbor, where water depths below the keel are often only 1 to 3 meters, the aft and forward sections of the ship will most likely come into contact with the channel bottom. This might actually help support and stabilize the LNG ship until a full damage assessment could be conducted. If the ship is at an offshore or Deepwater Port, the expected ship damage and deformation, without mitigation approaches and steps taken, could lead to a total loss of the LNG ship.

Since the remaining four cargo tanks were not breached during the initial event, and due to the fact that the cargo tanks are designed to contain the LNG independent of the hull structure, any additional release of LNG from the ship damage in a cascading progression, either simultaneously or consecutively, was judged to be unlikely. However, the ship will be disabled and incapable of transit, and likely require that the remaining cargo be removed in as prudent and timely a manner as possible for safety reasons.

As with the Moss LNG ship, the initial Summer Arrival stress state was computed for the Membrane ship, prior to assessing the regions exposed to an LNG spill. Again as with the Moss, because the flow analyses for the large to very large breach events and spills were similar, only one cryogenic structural damage analysis was conducted. These flow results were used to develop the cooled regions for the cryogenic damage analysis. Figures 24 and 25 show exterior and interior views of the ship's cooled regions respectively. Widespread LNG flow between the inner and outer hulls occurs within 2 and 3 minutes, with subsequent filling of the compartments. At approximately 6 to 10 minutes into the spill, a significant portion of the total ballast tank and areas between the inner and outer hulls are filled. While complete filling of the ballast compartments and areas between the double hulls does not occur, the open spaces are small and would contain cold LNG vapor and therefore, the entire ballast tank below the breach was included as one large cooled region.

The temperatures of the elements within the dark blue regions of Figure 24 and Figure 25 decreased from 20^{o}C to -148^{o}C over 10 minutes. Due to the time required for the flow to reach a significant portion of the cooled region, a better time estimate may be to add several minutes to the 10 minutes required for cooling the structural elements. Finally, the same assumptions were made for the Membrane ship as the Moss ship regarding cooling rates above and below the waterline and the eventual entrainment of seawater into the ship for some breach events and their inclusion in the damage conclusions.

Figure 26 shows the Membrane ship with temperatures and damage plotted. The white colored elements indicate the cryogenic fractures calculated after reaching the critical strain criterion during cooling. The transparent view shows both the cracking in the outer hull and inner hull surrounding the cargo tank. Here, the extent of the damage to vessel structure surrounding the breached cargo tank can be seen. The analysis predicts cracking will occur throughout the entire cooled region, which reflects those portions of the ship that were exposed to LNG flow.

The damage was predicted to occur primarily near the cooled region boundaries. This is likely an artifact of the sharp gradient from cool to warm material along this boundary. Once the cracks occurred in the structural model, these elements were removed, and much of the stress was reduced in the interior of the cooled region, preventing further apparent damage. The cryogenic fracture and cracking in an actual event is expected to extend throughout much of the cooled region, especially in areas of flaws or stress concentration such as welds, corrosion, etc. As with the Moss ship analysis, no damage was predicted to occur in regions outside of the cooled areas. The warm regions have a significantly higher fracture toughness and hence a higher strain to failure criterion.

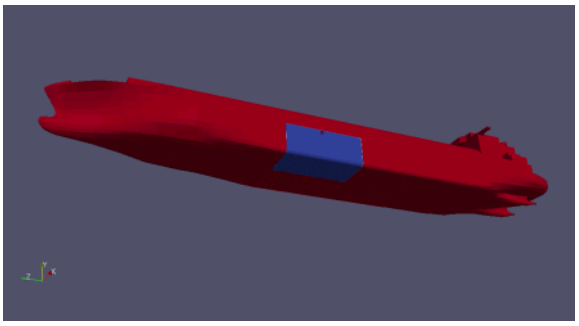

Figure 24. Membrane exterior regions of temperature decrease

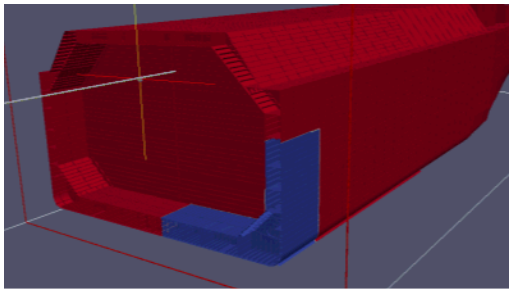

Figure 25. Membrane interior regions of temperature decrease

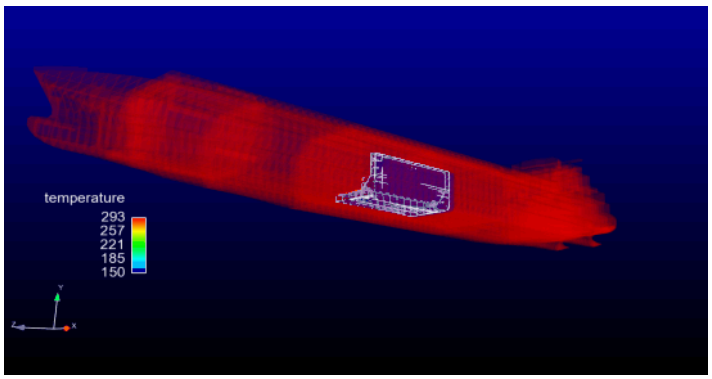

Figure 26. Example Membrane damage due to cryogenic LNG flow

Again, as with the Moss structural model, because of the severe cryogenic structural damage calculated, including a significant number of killed elements and separation of regions of elements, the numerical structural damage model became unstable. Therefore, assessing the final global ship deformation and response with this model after the cryogenic damage that was induced was not possible. The following section though uses the cryogenic damage calculated to provide a general overall assessment of the Membrane LNG ship damage from a large cargo tank breach, spill, and fire.

The effective damage to the Membrane ship is initially localized on one side of the ship. The majority of the inner and outer hull was damaged severely reducing the ability of the vessel to resist hydrostatic loads from the surrounding seawater. Unlike the Moss vessel, which has the LNG cargo tank structurally separated from the inner hull, the Membrane ship inner hull provides the structural support for the cargo tank. With the damage to the inner hull, the cargo tank in the affected region will likely not be capable of fully containing the LNG cargo that remains below the breach.

The cryogenic damage will reduce the ship structural moment of inertia, or section modulus (the parameter that defines the ship's capability to resist bending loads and deformations), and as discussed for the Moss ship,his will also impact the ability of the membrane ship to remain stable and afloat in the water. From the fire analysis, much of the ship structure near the fire on both the side and top of the Membrane ship could reach temperatures of between 775°C and 1000°C for the inner and outer hulls. At these temperatures, the material properties of ship structural steels were shown from our testing to be severely weakened, having less than 25 percent of their original strength, and to deform significantly. Since the inner and outer hulls provide the structural support for the Membrane cargo tanks, thermal degradation of the outer and inner hulls would likely damage cargo tanks impacted by a large LNG fire for long periods.

Based on the cryogenic and fire damage estimated, the reduced cross-sections and weakened material from the fire, the plastic bending moment capacity for the Membrane ship was computed as a function of time as shown in Figure 27. The plastic bending moment capacity is defined as the bending moment that would lead to the entire cross-section of the ship yielding and creating essentially a plastic "hinge". As mentioned with the Moss ship, the evaluation of the plastic bending moment capacity is often used in many extreme event risk analyses to more accurately predict the likelihood of overall structural system damage or failure during extreme events.

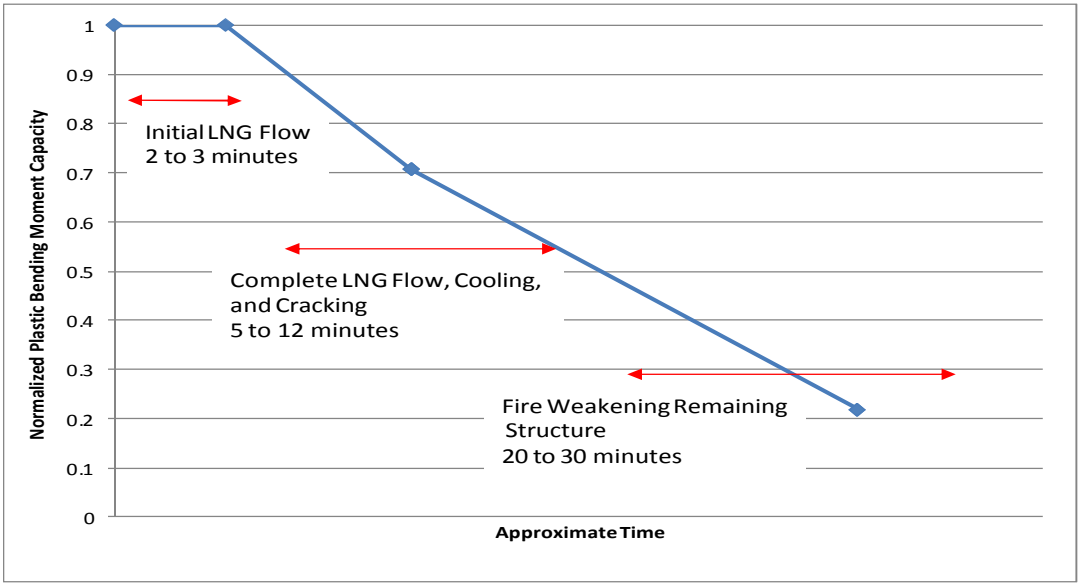

Figure 27. Membrane ship plastic bending moment capacity for large spills

The cryogenic damage causes an approximate 29% reduction within 5 to 12 minutes (including several minutes to account for the slower flow calculated for the Membrane ship design) with the fire causing an additional 50% reduction between 20 and 30 minutes. The fire has a more significant effect on the Membrane ship moment capacity due to the greater amount of remaining cross-section that is exposed to the fire as compared to the Moss. As with the Moss, the damage to the ship also introduces concerns related to the reduced buckling capacity for structural regions in compression. However, much of the inner and outer hulls in compression are in undamaged regions, making buckling less likely than for the Moss. The Membrane ship begins in a "sag" condition and transitions to a "hog" condition after the damage and loss of cargo in the breached center cargo tank. This would place the fire impacted regions in tension, where the material has little remaining strength. Therefore, the ship is judged to have essentially no remaining strength and the ship overall would be disabled and severely damaged.

As with the Moss ship, the Membrane ship will likely deform significantly or may even separate at the damaged tank region. However, these events are also assumed to occur in a near harbor location where the water depth below the keel is only on the order of 1 to 3 meters. Therefore, the aft and forward sections of the vessel will most likely come into contact with the seafloor.

Since the remaining four cargo tanks were not breached during the initial event, the release of their cargo is more uncertain. One of the tanks adjacent to the initially breached tank does experience cracking in the corner of the inner hull that was exposed to LNG as illustrated in Figure 28. The breach of this adjacent tank is possible, but not certain. Even so, if this adjacent tank were to experience a leak, it would most likely progress slowly and/or occur during the fire portion of the event when the fire would weaken the vessel structure in the adjacent tank. This would have the effect of extending the length of the fire, but not growing the size of the pool significantly.

As for the remaining tanks, one would likely be fully engulfed while the other two would be partially engulfed. From the fire analysis, the inner and outer hulls would be significantly weakened. Since the inner hull supports the cargo tank, this reduced strength could make a breach of another cargo tank possible. However, the cargo tank liner is very ductile and can deform significantly without tearing. Overall, the additional release of LNG in a *rapid* cascading progression was judged to be unlikely, though successive damage and LNG spills might be possible. This probably would not increase the size of a spill, but again could extend the length of a fire. However, the vessel will be disabled and incapable of transit and would require that the remaining cargo be removed in as timely a manner as possible.

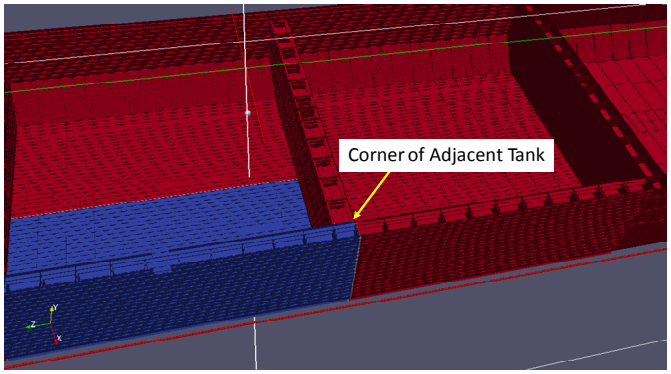

Figure 28. Membrane ship cracking in corner of adjacent tank

For the small breach events noted in Table 2, which could occur from a number of credible intentional events, the spill rates will be more than a factor of 1000 times less than that of the large breach events considered. This puts the associated smaller spills into a regime that would typically fall within current spill detection and safety systems on Moss and Membrane LNG ships. The large reduction in spill rates, cryogenic damage and fire damage potential suggests that Moss and Membrane LNG ships that would experience small breach events would have sufficient time to find an appropriate anchorage location and work with the local public safety agencies and the Coast Guard to determine appropriate damage assessment, safety, and possibly repair procedures.

The medium size breach sizes noted in Table 2, 0.5 m^2 (2.3 feet square) because of the physics of the flow conditions, will reduce the LNG flow rate into an LNG ship by a factor of approximately six, relative to a large LNG spill. As such, the full cryogenic cooling and damage of all the compartments between the LNG hulls for each ship could take as much as six times as long. But based on the flow analysis conducted for the medium holes, the LNG flow internal to the ship reaches the keels of the LNG ships only a few minutes later than the larger spills. This suggests that for the medium size breach events and spills, the full cryogenic damage could take from 10 minutes to no more than 60 minutes longer than for the larger spills. Unfortunately, the fire damage will still occur over the original time period calculated, and therefore the overall rate of reduction in structural capability will not be changed significantly. Therefore, a medium size breach event could double or triple the time before an LNG ship becomes disabled, but it would still occur in within an hour or so of the breach event and spill, which does not provide significant time to move the LNG ship to a safe anchorage.

VII. Conclusions

The significant findings and conclusions from the LNG cryogenic and fire thermal damage analysis are summarized below.

Summary Assessment of Moss LNG Ship Cryogenic and Fire Damage

- The structural integrity can be severely compromised for large spills with the majority of the inner hull cracked and no longer capable of effectively resisting any load.
- The fire loading reaches temperatures which would drastically reduce the strength of some of the steel structure.
- As mentioned above, the damage to the inner hull leaves the remaining outer hull in a state where it will buckle under local hydrostatic pressures let alone the global bending loads imposed by the remaining structure.
- The vessel in the region of the breach and spill will be severely damaged and will deform significantly and may lead to a separation of the vessel. If this occurs in a shallow harbor location, the vessel is likely to settle at the channel bottom.
- The remaining LNG in the cargo tank below the breach level will likely escape either due to a further rupture of the tank from global vessel deformation or due to the breach displacing below the waterline.
- Due to the independent nature of the LNG cargo tank structure from the surrounding vessel structure, the deformation of the ship is judged to be unlikely to cause a breach of adjacent cargo tanks, e.g., cause cascading damage.

Summary Assessment of Membrane LNG Ship Cryogenic and Fire Damage

- The structural integrity can be severely compromised for large spills with the inner and outer hulls cracked below the breach over one-half of the vessel. These cracked regions are no longer capable of effectively resisting any load.
- The remaining LNG in the cargo tank below the breach level will not be contained by the damaged inner hull below the spill due to the local cryogenic damage of the tank.
- The fire loading reaches temperatures that would drastically reduce the strength of the double hull structure. A significantly large percentage of the ship cross-section is subjected to fire degradation.
- The ship in the region of the breach is severely damaged by cracking and weakened by the fire and will deform significantly and may lead to a separation of the ship. If this event occurs in a shallow harbor location, the vessel is likely to settle to the bottom of the channel.
- One of the tanks adjacent to the breach tank will experience limited cracking of the inner hull. Since the inner hull is integral in maintaining containment of the LNG cargo, a leak in this tank is possible, especially after additional deformation of the tank due to heating from an external fire. This additional leakage was thought to be more likely later in the event after the LNG from the initial breach had been burned to near exhaustion. Therefore, any additional leakage of the LNG from the adjacent tank would extend the time of the fire but not the size of the pool.
- Due to the integral nature of the LNG cargo tank with the surrounding ship structure, the deformation of the ship structure surrounding the remaining cargo tanks due to the external fire could compromise the integrity of these tanks. However, the cargo tank liner material is ductile and any additional breaches of the adjacent tanks were judged to be unlikely to cause immediate simultaneous cascading damage, but could extend the length of the spill.

Overall Summary Results for Large and Very Large Breaches

- Both ships are judged to be disabled and severely damaged due to a large cargo tank breach and spill.
  Neither ship would be capable of movement and would need to have any remaining LNG cargo transferred.

Overall Summary Results for Medium Breaches

- Similar results as the large and very large breaches, just over a slightly longer time period (approximately 1 hour).
- The Moss and Membrane LNG ships would not likely have sufficient time to find an appropriate anchorage location prior to becoming disabled of severely damaged.

Overall Summary Results for Small Breaches

- For the small breach events, which could occur from a number of credible intentional events, the spill rates will be more than a 1000 times less than that of the large breach events considered.
- This puts the associated smaller spills into a regime that would typically fall within current spill detection and safety systems on Moss and Membrane LNG ships.
- The Moss and Membrane LNG ships would have sufficient time to find an appropriate anchorage location and work with the local public safety agencies and the Coast Guard to determine appropriate damage assessment, safety, and repair options.

VIII. References

Adaptive Research, (2008), CFD2000 - A general-purpose CFD program intended for complex scientific and engineering flow calculations), Keith Kevin O'Rourke.

Blanchat, T., Helmick, P., Jensen, R., Luketa, A., Deola, R., Suo-Anttila, S., Mercier, J., Miller, T., Ricks, A., Simpson, R., Demosthenous, B., Tieszen, S., and Hightower, M., (2010). *The Phoenix Series Large Scale LNG Pool Fire Experiments*, SAND2010-8676, Sandia National Laboratories, Albuquerque, NM.

Blanchat, T.(2011). *LNG Carrier Tank Insulation Decomposition Experiments with Large Scale Pool Fire Boundary Conditions*, SAND2011-1880, Sandia National Laboratories, Albuquerque, NM.

Figueroa, V.G., Lopez, C., O'Rourke, K.K., (2011). *LNG Cascading Damage Study Volume II: Flow Analysis for Spills from MOSS and Membrane LNG Cargo Tanks*, SAND2011-9464. Sandia National Laboratories, Albuquerque, NM.

GAO (2007). "Public Safety Consequences of a Terrorist Attack on a Tanker Carrying Liquefied Natural Gas Need Clarification," Government Accountability Office report, GAO -07-316, February 2007.

Hightower, M., et al. (2004). *Guidance on Risk Analysis and Safety Implications of a Large Liquefied Natural (LNG) Spill Over Water*, SAND2004-6258. Albuquerque, NM: Sandia National Laboratories.

Hightower, M., Luketa-Hanlin, A., Gritzo, L.A., Covan, J.M. (2006). *Review of Independent Risk Assessment of the Proposed Cabrillo Liquefied Natural Gas Deepwater Port Project*, SAND2005-7339, Sandia National Laboratories, Albuquerque, NM.

Kalan, R. J., Petti, J. P.(2010). *LNG Cascading Damage Study Volume I: Fracture Testing Report*, SAND2011-3342, Sandia National laboratories, Albuquerque, NM.

Luketa, A.J., M.M. Hightower, S. Attaway, (2008). *Breach and Safety Analysis of Spills over Water from Large Liquefied Natural Gas Carriers*, SAND2008-3153, Sandia National Laboratories, Albuquerque, NM.

Petti, J.P., Wellman, G.W., Villa, D., Lopez, C., Figueroa, V.G., Heinstein, M. (2011), *LNG Cascading Damage Study Volume III: Vessel Structural and Thermal Analysis Report*, SAND2011-6226, Sandia National Laboratories, Albuquerque, NM.